Shear viscosity of hadrons with K-matrix cross sections

Anton Wiranata,[1,2,*] Volker Koch,[2,†] Madappa Prakash,[3,‡] and Xin Nian Wang[1,2,§]
[1]*Institute of Particle Physics and Key Laboratory of Quark and Lepton Physics (MOE), Central China Normal University, Wuhan 430079, China*
[2]*Lawrence Berkeley National Laboratory, Nuclear Science Division, MS 70R0319, Berkeley, California 94720, USA*
[3]*Department of Physics and Astronomy, Ohio University, Athens, Ohio 45701, USA*
(Received 17 July 2013; published 28 October 2013)

Shear viscosity η and entropy density s of a hadronic resonance gas are calculated using the Chapman-Enskog and virial expansion methods using the K-matrix parametrization of hadronic cross sections which preserves the unitarity of the T matrix. In the π-K-N-η mixture considered, a total of 57 resonances up to 2 GeV were included. Comparisons are also made to results with other hadronic cross sections such as the Breit-Wigner (BW) and, where available, experimental phase shift parameterizations. Hadronic interactions forming resonances are shown to decrease the shear viscosity and increase the entropy density leading to a substantial reduction of η/s as the QCD phase transition temperature is approached.

DOI: 10.1103/PhysRevC.88.044917 PACS number(s): 25.75.Ld, 05.20.Dd, 47.75.+f, 51.20.+d

I. INTRODUCTION

Experimental data from high-energy nucleus-nucleus collisions at the Relativistic Heavy-Ion Collider (RHIC) [1–8] and the Large Hadron Collider (LHC) [9–18] indicate that a significant amount of collective flow is being developed during the partonic or quark-gluon plasma stage of the evolving system. The collective flow is manifested in particle spectra which are blue shifted and exhibit an anisotropy with respect to the event plane. The anisotropy in the spectra, which is often referred to as anisotropic flow, is due to collective expansion which converts the geometric anisotropy of the initial energy density distribution into anisotropic distribution in azimuthal angles of the detected hadrons. The observed anisotropic flow is typically characterized in terms of Fourier components, v_n. For noncentral collisions, the second moment v_2 dominates reflecting the shape of the overlapping nuclei at finite impact parameters. The higher Fourier components, on the other hand, are due to event-by-event fluctuations of the initial geometry [19]. These higher moments have been studied within event-by-event ideal and viscous hydrodynamical model calculations [20–25] with the finding that the they are mainly determined by fluctuations in the initial conditions, and the ratio of the shear viscosity η and entropy density s. Comparisons between experimental data and hydrodynamic calculations thus have the promise to provide increasingly stringent constraints on the η/s of the dense matter and the initial conditions [26–28].

First-principle calculations of the shear viscosity of strongly interacting matter from QCD over a large range of temperature have so far been elusive. However, model calculations of strongly interacting matter in different ranges of temperature can provide an interesting picture of the temperature dependence of the shear viscosity to entropy density ratio, η/s [29,30]. Based on experimental π-π shifts, calculations [31,32] give an η/s ratio for a pion gas that decreases with temperature as $\sim 1/T^4$ [33], whereas perturbative QCD calculations [34–39] predict a smaller η/s that increases logarithmically with temperature in a quark-gluon plasma. This ratio, believed to be bound by a limit of $1/(4\pi)$ (in units of $\hbar/k_B$) from Anti-de Sitter Space/Conformal Field Theory (AdS/CFT) calculations [40], likely reaches a minimum around the QCD phase transition temperature.

Lacking firm theoretical guidance on the temperature dependence of the η/s ratio, most hydrodynamic model studies have assumed a constant η/s, whereas some studies have incorporated hadronic cascade models (termed afterburners) [41,42] following hydrodynamic evolution in order to incorporate the effect of a large shear viscosity in the hadronic phase. A systematic study of shear viscosity to entropy density ratio in the hadronic phase is therefore important to assess the effects of transport properties throughout the evolution; that is, from of the quark-gluon plasma stage to the phase transition stage and thereafter the hadronic stage.

In this paper, we present our study of the shear viscosity to entropy density ratio in a hadronic resonance gas with 57 resonances (with masses up to 2 GeV taken from the Particle Data book) formed by interactions among the components of a π-K-N-η mixture. Our calculations are for a system with zero net baryon and strangeness numbers. Resonant interactions, including the widths of the various resonances, are incorporated consistently in calculations of both the shear viscosity and the entropy density. We employ the K-matrix parametrization of the hadronic cross sections which accommodates multiple resonances and preserves the unitarity of the T matrix in all channels. We show how the inclusion of multiple resonances in a multicomponent mixture decreases the shear viscosity to entropy density ratio η/s with increasing number of components in the mixture as the temperature approaches that of the QCD phase transition.

This paper is organized as follows. Our calculation of shear viscosity, carried out numerically within the Chapman-Enskog approximation, is reviewed in Sec. II. In Sec. III, we examine

*awiranata@lbl.gov
†vkoch@lbl.gov
‡prakash@phy.ohiou.edu
§xnwang@lbl.gov

 ©2013 American Physical Society

different parametrizations of differential cross sections that have been used in the calculation of transport cross sections needed for the calculation of shear viscosity. The thermodynamics of interacting hadrons using the virial expansion approach is discussed in Sec. IV. Analytical and numerical results are presented in Sec. V for a single-component gas of pions. Section VI contains results for the multicomponent π-K-N-η mixture. We summarize and conclude with an outlook in Sec. VI. The Appendices contain relevant details of the K Matrix, Breit-Wigner, and phase shift parametrizations of cross sections.

II. SHEAR VISCOSITY

We employ the Chapman-Enskog approach, generalized to include relativistic kinematics, for the calculation of shear viscosity. This approach enables us to consider a mixture in which particles with different masses give rise to multiple massive resonances through hadronic interactions. In the case of a single-component system, we follow closely the formalism developed in Refs. [43,44] considering only the number conserving elastic processes. In the case of binary and multicomponent mixtures, we adapt the formalism detailed in Refs. [44,45] to treat the hadronic gas composed of a large number of resonances. In the context of hadronic interactions, the procedure to calculate shear viscosity has also been described in detail in Refs. [32,46]. We present only the final results in this section and refer the reader to earlier works for details.

A. Single-component system

Here we summarize the working formulas relevant for a single-component gas consisting of hadrons with mass m. To first order, the shear viscosity is given by

$$\eta_s = \frac{1}{10}\, T\, \frac{\gamma_0^2}{c_{00}}, \quad \gamma_0 = -10\,\hat{h}, \quad \hat{h} = K_3(z)/K_2(z), \tag{1}$$

where $z = m/T$ is the relativity parameter, $\hat{h}$ is the reduced enthalpy per particle, and $K_\nu(z)$ is the modified Bessel function of order ν. The quantity c_{00} is given by

$$c_{00}(z) = 16\left[w_2^{(2)}(z) - w_1^{(2)}(z)/z + w_0^{(2)}(z)/(3z^2)\right], \tag{2}$$

where $w_i^{(s)}(z)$ are the so-called relativistic omega integrals:

$$w_i^{(s)}(z) = \frac{2\pi z^3}{K_2(z)^2}\int_0^\infty d\psi \sinh^7\psi \cosh^i\psi\, K_j(2z\cosh\psi) \times \int_0^\pi d\Theta \sin\Theta\, \sigma_{00}(\psi,\Theta)(1-\cos^s\Theta). \tag{3}$$

The differential cross section for interaction between two identical particles is given by $\sigma_{00}(\psi,\Theta)$, $j = 5/3 + 1/2(-1)^i$. Hyperbolic functions of the quantity ψ characterize the relative momentum and invariant center-of-mass energy of the two colliding particles:

$$\sinh\psi = \frac{g}{m}, \quad \cosh\psi = \frac{P}{2m}, \tag{4}$$

where $g = \sqrt{(p_1-p_2)^2}/2$, $P = \sqrt{(p_1+p_2)^2}$, and p_1 and p_2 are the initial four-momenta of the two colliding hadrons.

The Chapman-Enskog approach also allows us to improve upon the first-order result in Eq. (1). Expressions for higher orders can be found in Refs. [43,44]. Results obtained using higher-order approximations in the case of a pion gas with experimental cross sections have been presented earlier in Ref. [32], showing rapid convergence with respect to the order of the approximation.

B. Multicomponent system

1. Binary mixture

To first order, the shear viscosity in the case of a binary mixture is given by

$$\eta_s = \frac{1}{10}T\left[\frac{\gamma_2^2 c_{11} + \gamma_1^2 c_{22} - 2\gamma_1\gamma_2 c_{12}}{(c_{11}c_{22} - c_{12}^2)}\right], \tag{5}$$

where $\gamma_k = -10\,\tilde{x}_k\hat{h}_k$ $(k = 1,2)$ and $\hat{h}_k = K_3(z_k)/K_2(z_k)$ with $z_k = m_k/T$ being the reduced enthalpy per particle for particle type $k = (1,2)$ with mass m_k. The coefficients $\tilde{x}_k = \rho_k/\rho$ are related to the mass density ρ_k (mass times the number density) of particle type k and $\rho = \sum_k \rho_k$ is the total mass density. The coefficients c_{kl} are given by

$$c_{kk} = c_{00}(z_k) + \tilde{c}_{kk}(kl), \tag{6}$$

$$c_{kl} = \tilde{c}_{kl}(kl), \quad \text{for} \quad k \neq l, \tag{7}$$

where the coefficients $\tilde{c}_{kl}(kl) = \tilde{c}_{lk}(lk)$ are used to denote contributions to the shear viscosity from interactions between different particle species (1–2 for a binary mixture), while $c_{00}(z_k)$ accounts for contributions from interaction between two identical particles of type k. The corresponding coefficients $\tilde{c}_{kl}(kl)$ are by given by

$$\begin{aligned}\tilde{c}_{12} = \frac{32\rho^2\tilde{x}_1^2\tilde{x}_2^2}{3M_{12}^2 n^2 x_1 x_2}\big[&-10 z_1 z_2 \zeta_{12}^{-1} Z_{12}^{-1} w_{1211}^{(1)}(\sigma_{12}) \\ &- 10 z_1 z_2 \zeta_{12}^{-1} Z_{12}^{-2} w_{1311}^{(1)}(\sigma_{12}) + 3 w_{2100}^{(2)}(\sigma_{12}) \\ &- 3 Z_{12}^{-1} w_{2200}^{(2)}(\sigma_{12}) + Z_{12}^{-2} w_{2300}^{(2)}(\sigma_{12})\big],\end{aligned} \tag{8}$$

$$\begin{aligned}\tilde{c}_{11} = \frac{32\rho^2\tilde{x}_1^2\tilde{x}_2^2}{3M_{12}^2 n^2 x_1 x_2}\big[&10 z_1^2 \zeta_{12}^{-1} Z_{12}^{-1} w_{1220}^{(1)}(\sigma_{12}) \\ &+ 10 z_1^2 \zeta_{12}^{-1} Z_{12}^{-2} w_{1320}^{(1)}(\sigma_{12}) + 3 w_{2100}^{(2)}(\sigma_{12}) \\ &- 3 Z_{12}^{-1} w_{2200}^{(2)}(\sigma_{12}) + Z_{12}^{-2} w_{2300}^{(2)}(\sigma_{12})\big],\end{aligned} \tag{9}$$

$$\begin{aligned}\tilde{c}_{22} = \frac{32\rho^2\tilde{x}_1^2\tilde{x}_2^2}{3M_{12}^2 n^2 x_1 x_2}\big[&10 z_2^2 \zeta_{12}^{-1} Z_{12}^{-1} w_{1202}^{(1)}(\sigma_{12}) \\ &+ 10 z_2^2 \zeta_{12}^{-1} Z_{12}^{-2} w_{1302}^{(1)}(\sigma_{12}) + 3 w_{2100}^{(2)}(\sigma_{12}) \\ &- 3 Z_{12}^{-1} w_{2200}^{(2)}(\sigma_{12}) + Z_{12}^{-2} w_{2300}^{(2)}(\sigma_{12})\big],\end{aligned} \tag{10}$$

where $x_k = n_k/n$, n_k is the particle number density of particle type k, and $n = \sum_k n_k$ is the total particle number density. We have denoted the summed mass by $M_{kl} = m_k + m_l$ and the reduced mass by $\mu_{kl} = m_k m_l/M_{kl}$ for two nonidentical particles $(k \neq l)$. Additionally, $\zeta_{kl} = 2\mu_{kl}/T$ and $Z_{kl} = M_{kl}/2T$.

The relativistic omega integrals for a binary mixture are given by

$$w^{(s)}_{rtuv}(\sigma_{kl}) = \frac{\pi\,\mu_{kl}}{4\,T\,K_2(z_k)\,K_2(z_l)} \int_0^\infty d\Psi_{kl}\,\sinh^3\Psi_{kl} \times \left(\frac{g^2_{kl}}{2\mu_{kl}T}\right)^r \left(\frac{M_{kl}}{P_{kl}}\right)^t (\cosh\psi_k)^u (\cosh\psi_l)^v \times K_n\left(\frac{P_{kl}}{T}\right) \int_0^\pi d\Theta_{kl}\,\sin\Theta_{kl}\,\sigma_{kl}(\Psi_{kl},\Theta_{kl}) \times (1-\cos^s\Theta_{kl}), \tag{11}$$

where

$$P^2_{kl} = m^2_k + m^2_l + 2m_k m_l \cosh\Psi_{kl}, \tag{12}$$

$$g_{kl}P_{kl} = m_k m_l \sinh\Psi_{kl}, \quad \Psi_{kl} \equiv \psi_k + \psi_l, \tag{13}$$

$$\cosh\psi_k = \frac{1}{P_{kl}}(m_k + m_l\cosh\Psi_{kl}), \tag{14}$$

$$\cosh\psi_l = \frac{1}{P_{kl}}(m_l + m_k\cosh\Psi_{kl}), \tag{15}$$

with $P_{kl} = \sqrt{(p_k+p_l)^2}$ and $g_{kl} = \sqrt{(p_k-p_l)^2}/2$ characterizing the invariant center-of-mass energy and relative momentum of two particles with initial four-momenta p_k and p_l. In the case of $m_k = m_l = m_i$, $\Psi_{ii} = 2\psi_i$, $P_{ii} = 2m_i\cosh\psi_i$ and the relativistic omega integral for binary mixture reduces to Eq. (3).

2. Tertiary and higher component mixtures

In a mixture containing N components ($k, l = 1, 2, \ldots, N$), the first-order coefficient of shear viscosity within the Chapman-Enskog approximation is given by

$$\eta_s = \frac{1}{10}\rho^2 T^3 \sum_{k=1}^N \sum_{l=1}^N c_k\,c_l\,c_{kl}, \tag{16}$$

where c_k are coefficients of the orthogonal Laguere polynomials used as an ansatz function in solving for the coefficient of shear viscosity (for details, see Refs. [45,47]). The additional sum rule required to solve for c_k in terms of c_{kl} and γ_k is given by

$$\sum_{l=1}^N \left(\frac{\rho\,T}{n}\right)^2 c_l\,c_{kl} = \frac{\rho\,T}{n^2}\,\gamma_k, \tag{17}$$

where $k, l = 1, 2, \ldots, N$ (the number of particle species).

As for the single-component gas and for the binary mixture, the coefficients c_k are linear combinations of γ_k and c_{kr}. Thermodynamic variables are hidden in the coefficients γ. Interactions among particles in the mixture given in terms of differential cross sections reside in the omega integrals, and the coefficients c_{kr} are linear combinations of the omega integrals [45]. Explicitly, the required coefficients can be written as

$$c_{kk} = 16\,\tilde{x}^2_k\left(w^{(2)}_2(\sigma_{kk}) - \frac{1}{z}\,w^{(2)}_1(\sigma_{kk}) + \frac{1}{3z}w^{(2)}_0(\sigma_{kk})\right) + \sum_{l\neq k}^N \frac{32\rho^2\tilde{x}^2_k\tilde{x}^2_l}{3M^2_{kl}n^2x_kx_l}\big[10z^2_k\zeta^{-1}_{kl}Z^{-1}_{kl}w^{(1)}_{1220}(\sigma_{kl}) + 10z^2_k\zeta^{-1}_{kl}Z^{-1}_{kl}w^{(1)}_{1320}(\sigma_{kl}) + 3\,w^{(2)}_{2100}(\sigma_{kl}) - 3Z^{-1}_{kl}w^{(2)}_{2200}(\sigma_{kl}) + Z^{-1}_{kl}w^{(2)}_{2300}(\sigma_{kl})\big] \tag{18}$$

$$\tilde{c}_{kl} = \frac{32\rho^2\tilde{x}^2_k\tilde{x}^2_l}{3M^2_{kl}n^2x_kx_l}\big[-10z_kz_l\zeta^{-1}_{kl}Z^{-1}_{kl}w^{(1)}_{1211}(\sigma_{kl}) - 10z_kz_l\zeta^{-1}_{kl}Z^{-2}_{kl}w^{(1)}_{1311}(\sigma_{kl}) + 3w^{(2)}_{2100}(\sigma_{kl}) - 3Z^{-1}_{kl}w^{(2)}_{2200}(\sigma_{kl}) + Z^{-2}_{kl}w^{(2)}_{2300}(\sigma_{kl})\big] \quad (k\neq l). \tag{19}$$

The first of the above equations, Eq. (18), tells us how similar particles interact in the presence of other types of particles, whereas the second equation, Eq. (19), tells us how dissimilar particles interact in the mixture.

III. CROSS SECTION PARAMETRIZATIONS

The magnitude of shear viscosity is strongly determined by the strength of interactions between the constituent particles in a system. As is evident from Eqs. (1)–(3), the shear viscosity is inversely proportional to the differential cross section of the interacting particles. Large cross sections, characteristic of a strongly interacting system, naturally lead to small viscosities. In this work, we focus on shear viscosities in the hadronic phase of the strongly interacting matter that is created at RHIC/LHC. For all but the lightest particles, first-principle calculations of hadronic interactions, particularly those involving massive resonances, do not exist. One therefore often uses empirical parametrizations of these hadronic cross sections. To assess the impact of different parametrizations on the shear viscosity, we examine three forms of parametrizations: (i) cross sections obtained directly from the phase shifts [32,48], (ii) the Breit-Wigner parametrization for Ref. [49], and (iii) cross sections from the K-matrix [50] parametrization.

A. Cross sections from π-π phase shifts

A pion gas represents a good test case in which the role of resonances on the viscosity is exemplified. Experimentally, π-π shifts are available at least in three channels. The impact of additional channels for which phase shifts are not available will be considered in a subsequent section. For practical and illustrative purposes, we follow the parametrization employed by Bertsch *et al.* [48], which was used in the calculation of the shear viscosity of a pion gas in Ref. [32]. In terms of phase shifts, the differential cross section can be parameterized by

$$\sigma(\sqrt{s},\theta) = \frac{4}{q^2}\sum_{l+I=\text{even}} \frac{(2I+1)(2l+1)}{\sum_I(2I+1)} \times P^2_l(\cos\theta)\,\sin^2\delta^I_l(\sqrt{s}), \tag{20}$$

where l is the orbital angular momentum, I is the isospin, and the summation is over both l and I for $l+I$ being even numbers. The phase shift δ^0_0, corresponding to the σ resonance, is well fit by

$$\delta^0_0 = \frac{\pi}{2} + \arctan\left(\frac{\sqrt{s}-m_\sigma}{\Gamma_\sigma/2}\right), \quad \Gamma_\sigma = 2.06\,q, \tag{21}$$

where $m_\sigma = 5.8 m_\pi$ is the mass of the σ resonance, m_π is the pion mass, $\sqrt{s}$ is the center-of-mass energy, and $q = \sqrt{s - 4m_\pi^2}/2$ is the center-of-mass momentum of two colliding pions. The phase shift δ_0^2 corresponds to the repulsive channel and is given by

$$\delta_0^2 = -0.12\,\frac{q}{m_\pi}. \tag{22}$$

The phase shift δ_1^1 corresponds to the ρ resonance and is expressed by

$$\delta_1^1 = \frac{\pi}{2} + \arctan\left(\frac{E - m_\rho}{\Gamma_\rho/2}\right), \tag{23}$$

$$\Gamma_\rho = 0.095\,q\left[\frac{q/m_\pi}{(1+(q/m_\rho)^2)}\right]^2, \tag{24}$$

where $m_\rho = 5.53 m_\pi$ is the mass of the ρ resonance. Including contributions from $l = 0, 1, 2$, the differential cross section is then

$$\sigma(\sqrt{s},\theta) = \frac{4}{q^2}\left(\frac{1}{9}\sin^2\delta_0^0 + \frac{5}{9}\sin^2\delta_0^2 + 3\,\sin^2\delta_1^1\cos^2\theta\right). \tag{25}$$

These three phase shifts and the total cross section are shown in Fig. 1 as functions of center-of-mass momentum and energy, respectively.

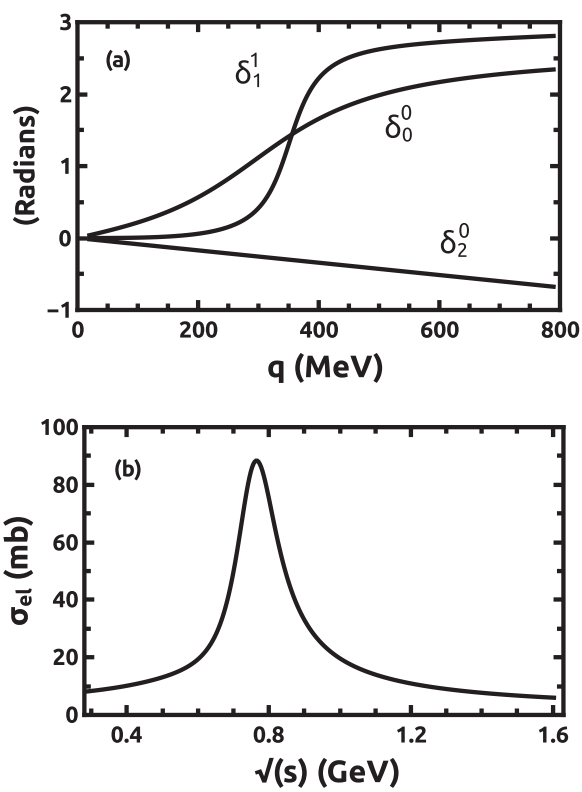

FIG. 1. (a) π-π phase shifts vs center-of-mass momentum from Eqs. (21)–(23). (b) Total cross section vs center-of-mass energy from Eq. (25).

B. The Breit-Wigner parametrization

The interaction or T matrix for hadronic interaction through a single resonance ($a + b \to R \to a + b$) can also be parameterized in the Breit-Wigner form [51] as

$$T = \frac{m_R\Gamma_{R\to ab}(\sqrt{s})}{(m_R^2 - s) - i m_R \Gamma_R^{\rm tot}(\sqrt{s})}. \tag{26}$$

where $\Gamma_R^{\rm tot} = \sum_{c,d}\Gamma_{R\to cd}$ is the total width and $\Gamma_{R\to ab}$ is the partial width for the channel $R \to ab$ of the resonance R, respectively. The differential cross section for such an interaction is then

$$\sigma(\sqrt{s},\theta) = \frac{C(I,l)}{q_{ab}^2}\,\frac{m_R^2\Gamma_{R\to ab}^2}{(m_R^2 - s)^2 + m_R^2\Gamma_R^{\rm tot^2}}P_l(\cos\theta) \approx \frac{C(I,l)}{q_{ab}^2}\,\frac{\Gamma_{R\to ab}^2}{4(m_R - \sqrt{s})^2 + \Gamma_R^{\rm tot^2}}P_l(\cos\theta), \tag{27}$$

where $C(I,l)$ is the symmetry factor which contains the spin-isopin multiplicities for the corresponding resonance, and q_{ab} is the center-of-mass momentum. The general cross section for the reaction $a + b \to c + d$ is then obtained by integrating over the polar angle and summing over all relevant resonances,

$$\sigma(\sqrt{s})_{a+b\to c+d} = \sum_R \frac{2S_R + 1}{(2S_a+1)(2S_b+1)}\,\frac{\pi}{q_{ab}^2} \times \frac{\Gamma_{R\to ab}\Gamma_{R\to cd}}{(m_R - \sqrt{s})^2 + \Gamma_R^{\rm tot^2}/4}, \tag{28}$$

where I denotes the isospin, I_3 is the third component of the isospin, and S is the spin for hadrons and resonances. The coefficients with angular brackets are the Clebsch-Gordon coefficients for the isospin. The center-of-mass momentum of the incoming particles is

$$q_{ab}(\sqrt{s}) = \frac{1}{2\sqrt{s}}\sqrt{[s - (m_a + m_b)^2][s - (m_a - m_b)^2]}, \tag{29}$$

and the energy dependence of the width in a given channel is typically given by

$$\Gamma_{R\to ab}(\sqrt{s}) = \Gamma_{R\to ab}^0\,\frac{m_R}{\sqrt{s}}\left(\frac{q_{ab}(\sqrt{s})}{q_{ab}(m_R)}\right)^{2l+1}\frac{1.2}{1 + 0.2\left(\frac{q_{ab}(\sqrt{s})}{q_{ab}(m_R)}\right)^{2l}}, \tag{30}$$

where m_R is the mass of the resonance, $\Gamma_{R\to ab}^0$ is the width for the channel $R \to ab$ at the pole, and l is the orbital angular momentum of the exit (decay) channel. Values for the resonance masses and their decay widths at the pole can be found in the Review of Particle Physics [51]. The last term in the above equation is related to the Blatt-Weisskopf B factor which can be found in Ref. [52].

C. The K-matrix parametrization

The K-matrix formalism [50,53,54] preserves unitarity of the T matrix for processes of the type $ab \to cd$. In this section, we provide a brief summary following closely the exposition in Ref. [50]. The differential cross section for $ab \to cd$ is

given in terms of the invariant amplitude $\mathcal{M}$ (or the scattering amplitude f) as

$$\sigma(\sqrt{s},\theta) = \frac{1}{(8\pi)^2 s}\left(\frac{q_{cd}}{q_{ab}}\right)|\mathcal{M}|^2 = |f(\sqrt{s},\theta)|^2, \tag{31}$$

where q_{ab} (q_{cd}) is the breakup momentum in the initial (final) state, θ is the usual polar angle in spherical coordinates, and $\sqrt{s}$ is the center-of-mass energy. The scattering amplitude $f(\theta)$ can be expressed as

$$f(\sqrt{s},\theta) = \frac{1}{q_{ab}}\sum_l (2l+1)\,T^l(s)\,P_l(\cos\theta), \tag{32}$$

in terms of the interaction matrix $T^l(s)$. The Legendre polynomials $P_l(\cos\theta)$ account for the angular momentum dependence of the exit channel.

In general, the T matrix can be defined from the overlap matrix between the initial and final states of the collision:

$$S_{ab\to cd} = \langle cd|S|ab\rangle, \quad S = I + 2i\,T, \tag{33}$$

where S is the scattering operator (matrix) and I is the identity operator accounting for no interaction. Based on the unitarity of the S matrix,

$$S\,S^\dagger = S^\dagger\,S = I, \tag{34}$$

one can arrive at the relation

$$(T^{-1} + iI)^\dagger = T^{-1} + iI. \tag{35}$$

Therefore, one can define a Hermitian K matrix through

$$K^{-1} = T^{-1} + iI, \quad K = K^\dagger. \tag{36}$$

Time-reversal symmetry of S and T also leads to K being symmetric. Therefore, the K matrix can be chosen to be real and symmetric. One can rewrite the T matrix in terms of the K matrix as

$$\begin{aligned}\mathrm{Re}\,T &= (I+K^2)^{-1}K = K(I+K^2)^{-1},\\ \mathrm{Im}\,T &= (I+K^2)^{-1}K^2 = K^2(I+K^2)^{-1}.\end{aligned} \tag{37}$$

In the K-matrix formalism, resonances appear as a sum of poles in the K matrix:

$$K_{ab\to cd} = \sum_R \frac{g_{R\to ab}(\sqrt{s})g_{R\to cd}(\sqrt{s})}{m_R^2 - s}, \tag{38}$$

where the sum on R goes over the number of resonances with masses M_R. The decay couplings are given by

$$g^2_{R\to ab}(\sqrt{s}) = m_R\Gamma_{R\to ab}(\sqrt{s}), \tag{39}$$

where the partial decay widths are given by

$$\Gamma_{R\to ab}(\sqrt{s}) = \Gamma^0_{R\to ab}\frac{m_R}{\sqrt{s}}\frac{q_{ab}}{q_{ab0}}[B^l(q_{ab},q_{ab0})]^2 \tag{40}$$

with $q_{ab0} = q_{ab}(m_R)$ being the breakup momentum at $\sqrt{s} = M_R$ and Γ^0 the width at the pole, as defined previously. The $B^l(q,q_0)$ is the usual Blatt-Weisskopf barrier factors which can be written in terms of the breakup momentum in channel $R\to ab$ and the resonance breakup momentum q_{ab} for the orbital angular momentum l:

$$B^l_{R\to ab}(q_{ab},q_{ab0}) = \frac{F_l(q_{ab})}{F_l(q_{ab0})}. \tag{41}$$

The list of $F_l(q)$ for $l = 0$ through 4 reads as

$$\begin{aligned}&F_0(q) = 1, \quad F_l(1) = 1,\\ &F_1(q) = \sqrt{\frac{2z}{z+1}}, \quad F_2(q) = \sqrt{\frac{13z^2}{(z-3)^2+9z}}\\ &F_3(q) = \sqrt{\frac{277z^3}{z(z-5)^2+9(2z-5)}}, \quad \text{and}\\ &F_4(q) = \sqrt{\frac{12746z^4}{(z^2-45z+105)^2+25z(2z-21)^2}},\end{aligned} \tag{42}$$

where $z = (q/q_R)^2$ and $q_R = 0.1973$ GeV/c. For interaction with a single resonance in the intermediate state, one can verify that the Breit-Wigner and K-matrix parametrizations are identical. We will explore their differences for the case of multiple and, especially, overlapping resonances later in this section.

D. Comparisons

In this subsection, we first compare results of total cross sections from three different parametrizations as described in the previous subsection for the $\pi\pi \to \rho \to \pi\pi$ channel. Thereafter, we include other resonances in $\pi\pi$ reactions in our comparisons. Finally, a discussion in the case of overlapping resonances is provided.

1. Single resonance

For interaction through a single resonance, the Breit-Wigner (BW) and K-matrix (KM) parametrizations are nearly identical. We will compare them to the phase-shift (PS) parametrizations here. Similar to the partial wave decomposition of the T matrix,

$$T = e^{i\delta_l}\sin\delta_l, \tag{43}$$

one can relate the phase shift in a single resonance channel to the K matrix,

$$K = \frac{m_\rho\,\Gamma_{\rho\to\pi\pi}(\sqrt{s})}{m_\rho^2 - s} = \tan\delta_l \tag{44}$$

for the process $\pi\pi \to \rho \to \pi\pi$. In Fig. 2, we compare the phase shift from BW/KM and PS parametrizations from Eq. (23). We used $m_\rho = 0.77$ GeV and the $\Gamma^0_{\rho\to\pi\pi} = 0.15$ GeV. The symmetry factor $C(I,l)$ is the same for all formalisms. While there is good agreement between the different parametrizations near the peak of the resonance, some differences exist at threshold and high energies because of the differences in the parametrizations of the widths between the PS and KM/BW approaches.

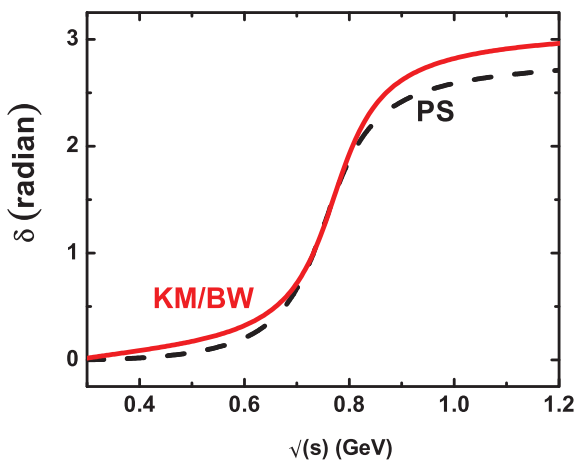

FIG. 2. (Color online) Phase shifts for $\pi\pi \to \rho \to \pi\pi$ from experiment as parametrized in Eq. (23) and from the K matrix of Eq. (44).

As discussed in Appendices A and B, all three parametrizations lead to identical cross sections if the same energy dependence of the decay width (Γ_ρ) is employed.

As we can see from the Argand diagram in Fig. 3, both the KM and BW parametrizations for a single resonance maintain the unitarity of the T matrix.

In Fig. 4, we show how a fit to the experimental cross sections that includes all three phase shifts compares with the KM/BW cross sections when only the ρ resonance is included. In the results shown, the fit to the experimental cross sections is isospin averaged. By using the appropriate symmetry factor, one is able to get the same result as that in the BW cross section.

In Fig. 4, we also compare the total cross sections from BW/KM parametrizations (solid curve), the PS parametrization with the ρ resonance only (dot-dashed), and the PS parametrization with the σ and ρ resonances together with the repulsive channel (dashed). While cross sections from BW/KM and PS for a single resonance are very similar around the resonance peak, there are significant differences near the threshold and at higher energies. The inclusion of the σ resonance and the repulsive channel in the PS parametrization significantly reduces the cross section at the resonance peak.

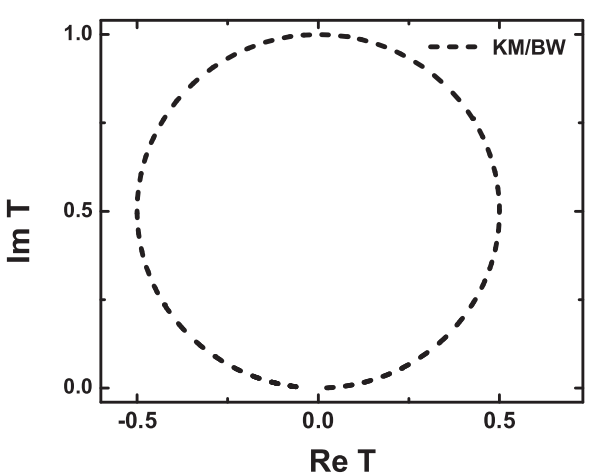

FIG. 3. The Argand plot of the T matrix for the $\pi\pi \to \rho \to \pi\pi$ calculated from the K-matrix and Breit-Wigner formalisms.

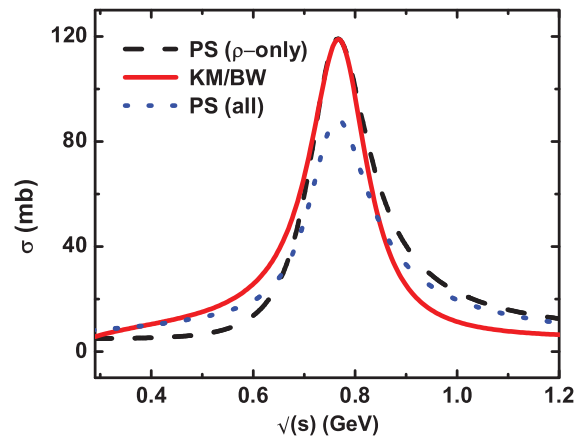

FIG. 4. (Color online) Total cross sections from phase shift fits, and from the Breit-Wigner/Urqmd and K-matrix formalisms.

2. *Separated and overlapping resonances*

In the case of two resonances, such as $a + b \to (m_\alpha, m_\beta) \to a + b$, the K matrix can be written as [50]

$$K = \frac{m_\alpha \Gamma_{\alpha\to\pi\pi}(\sqrt{s})}{m_\alpha^2 - s} + \frac{m_\beta \Gamma_{\beta\to\pi\pi}(\sqrt{s})}{m_\beta^2 - s}. \tag{45}$$

One can then calculate the T matrix from Eq. (37) and the total cross section from Eq. (31). One can also calculate the total cross section from the BW parameterization from Eq. (27). To illustrate the scenario when the two resonances are well separated (i.e., when the wings do not significantly overlap), we consider the first resonance with the mass of $m_\alpha = 1.2$ GeV with a width $\Gamma_\alpha = 0.1$ GeV, and the second resonance $m_\beta = 1.5$ GeV with a width $\Gamma_\beta = 0.2$ GeV. The total cross section for scattering of particles via these two resonances is shown in the left panel of Fig. 5. In this case, cross sections from the KM and BW parametrizations are very similar for most colliding energies, but the magnitude of the total cross section from the BW parametrization at the peak of the first resonance is slightly larger than that from the KM parametrization. This is because in BW the tail of the second resonance contributes to the peak of the first resonance, which is not the case for the KM.

We show the Argand plot of the T matrices for both parametrizations in the left panel of Fig. 6. The T matrix from the KM is able to maintain its unitarity whereas that from the BW is unable preserve this property exactly.

For two overlapping resonances, we consider $m_\alpha = 1.35$ GeV with $\Gamma_\alpha = 0.3$ GeV, and $m_\beta = 1.5$ GeV and $\Gamma_\beta = 0.1$ GeV. The total cross sections for the KM and BW cases are shown in the right panel of Fig. 5. We can see that the total cross section from the BW parametrization is generally larger than that from the KM parametrization. The difference is most significant around the peaks of the two resonances and also in the region between. Such a difference is caused by the contribution from the tail of one resonance to the peak region

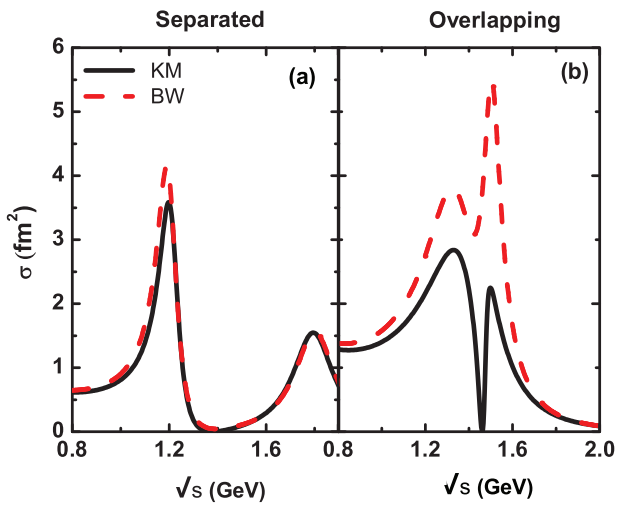

FIG. 5. (Color online) (a) Total cross sections for separated resonances m_α (1200) and m_β (1800). The widths are $\Gamma_\alpha = 0.1$ GeV and $\Gamma_\beta = 0.2$ GeV. (b) Total cross sections for nearby resonances m_α (1300) with $\Gamma_\alpha = 0.3$ GeV and m_β (1500) with $\Gamma_\beta = 0.1$ GeV. The solid line is the calculation from the K matrix (KM) parametrization and the dashed line is the calculation from the Breit-Wigner (BW) parametrization.

of another in the BW parametrization. Such contributions are absent in the KM parametrization.

In the right panel of Fig. 6, we show the T matrices from both the KM and BW parametrizations. The unitarity of the T matrix is preserved in the case of the KM formalism whereas such is not the case in the BW parametrization.

To conclude this section, we have shown that (i) for interaction through a single resonance, both KM and BW parameterization can maintain the unitarity of their T matrices, and the total cross sections are very similar to that from the PS parametrization; (ii) when an interaction contains multiple resonances, only the KM formalism is able to maintain the unitarity of the T matrix; and (iii) in the case of multiple resonances, the total cross section from the BW is always larger than that from the KM parametrization. In this work, we employ the KM parametrization to calculate the differential cross sections needed for the calculation of viscosity and the phase shifts required for the calculation of entropy density. Resonance masses and widths are taken from the Particle Data Group (PDG) [55]. Although the number of instances in which interference effects are significant is small, the use of the KM parametrization automatically guarantees the preservation of unitarity.

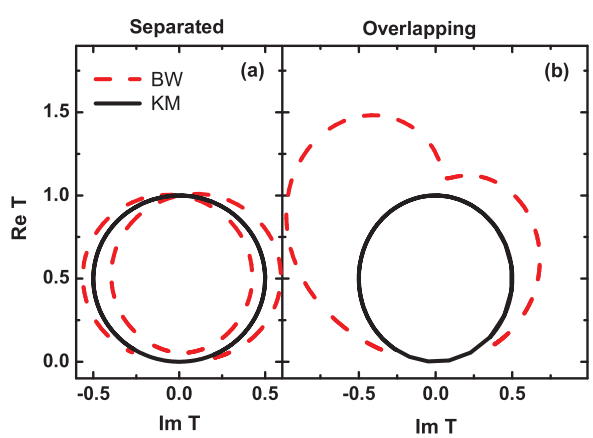

FIG. 6. (Color online) Argand diagrams of the T matrices corresponding to the resonances in (a) and (b) of Fig. 5. The solid line is the calculation from the K-matrix (KM) parametrization and the dashed line is the calculation from the Breit-Wigner (BW) parametrization.

IV. THERMODYNAMICS OF INTERACTING HADRONS

The equilibrium thermal properties of a hadron gas consists of ideal (from translational degrees of motion due to thermal agitation) and interacting (from strong interaction dynamics) parts. The ideal gas contributions are straightforward to compute (see, for example, the formulas in Appendix 1 of Ref. [56]). Leading contributions to the thermal properties from interactions between hadrons can be calculated using the second virial coefficient which can be deduced from two-body phase shifts [57]. The relativistic virial expansion introduced by Dashen *et al.* [58] has been fruitfully employed to calculate the state variables of interacting hadrons in Refs. [56,59], which we adopt in the following. Explicitly, interacting contributions to the pressure, energy density, and entropy density at the second virial level are given by the following expressions:

$$n_{\rm int} = \frac{1}{\pi^3}\int_M^\infty d\epsilon\, \epsilon^2 K_1(\epsilon\,\beta)\sideset{}{'}\sum_{l,I} g_l^I \delta_l^I(\epsilon), \tag{46}$$

$$P_{\rm int} = \frac{1}{\beta}\frac{1}{2\pi^3}\int_M^\infty d\epsilon\, \epsilon^2\, K_1(\epsilon\beta)\sideset{}{'}\sum_{l,I} g_l^I \delta_l^I(\epsilon), \tag{47}$$

$$\mathcal{E}_{\rm int} = \frac{1}{4\pi^3}\int_M^\infty d\epsilon\, \epsilon^3[K_2(\epsilon\beta)+K_0(\epsilon\beta)]\sideset{}{'}\sum_{l,I} g_l^I \delta_l^I(\epsilon), \tag{48}$$

$$s_{\rm int} = \beta\frac{1}{2\pi^3}\int_M^\infty d\epsilon\, \epsilon^3\, K_2(\epsilon\beta)\sideset{}{'}\sum_{l,I} g_l^I \delta_l^I(\epsilon), \tag{49}$$

where $M = m_a + m_b$ is the invariant mass of the interacting pair at threshold, $\beta = 1/T$, K_ν is the modified Bessel function of order ν, and $\epsilon = (q^2+m_a^2)^{1/2} + (q^2+m_b^2)^{1/2}$ is the total center-of-mass energy, q being the center-of-mass momentum of one of the two outgoing particles. The prime denotes that, for a given l, the sum over I is restricted to values consistent with statistics $(I+l)$ that are even; $g_l^I = (2l+1)(2I+1)$ is the spin-isospin degeneracy of the (l, I) resonance.

It is worthwhile mentioning here that contributions from higher than the second virial coefficient can significantly contribute to the state variables mentioned above. In general, the logarithm of the partition function can be written as

$$\ln Z = \ln Z_0 + \sum_{i_1,i_2} z_1^{i_1} z_2^{i_2} b(i_1, i_2), \tag{50}$$

where $z_j = \exp(\beta\mu_j)$ for $j = 1, 2$ are the fugacities and the virial coefficients $b(i_1, i_2)$ are [58]

$$b(i_1, i_2) = \frac{V}{4\pi i}\int \frac{d^3P}{(2\pi)^3}\int d\epsilon \exp(-\beta(P^2+\epsilon^2)^{1/2}) \times \left[A\left\{S^{-1}\frac{\partial S}{\partial \epsilon} - \frac{\partial S^{-1}}{\partial \epsilon}S\right\}\right]_c. \quad (51)$$

In the above, V, P, and ϵ stand for the volume, the total center-of-mass momentum, and energy, respectively. The labels i_1 and i_2 refer to a channel of the S matrix which has an initial state containing $i_1 + i_2$ particles; the trace is therefore over all combinations of particle number. The symbol A denotes the symmetrization (anti symmetrization) operator for a system of bosons (fermions) and the subscript c refers to the trace of all linked diagrams. The lowest (second) virial coefficient $b_2 \equiv b(i_i, i_2)/V$ as $V \to \infty$ corresponds to the case in which $i_1 = i_2 = 1$, from which the expressions in Eqs. (46)–(49) ensue. To our knowledge, multiparticle initial states—as would be appropriate, for example, to treat the $\omega(783)$ meson appropriately—have not been attempted thus far (including this work) in calculations of thermodynamics. The work of Lu and Moore [60], performed in the context of bulk viscosity, and in which the T matrix for three pions in the initial state was proposed, could be a starting point for investigating the role of the third virial coefficient.

An adequate treatment of repulsive channels and inelastic channels also requires careful attention. For all but the lightest mesons (π and K) and nucleons, experimental knowledge about repulsive interactions is not available. Since the interacting contributions to the state variables are given by a convolution of the isospin-weighted sum of the phase shifts with thermal weights, the repulsive channels negate the positive contributions of some of the attractive channels [56]. Furthermore, several reactions are characterized by significant amounts of inelasticities. While a complete knowledge of the T matrix would include inelastic channels, a practical approach that encompasses all the resonances encountered in a heavy-ion collision is yet to be devised. In this work, however, we will limit ourselves to the level of the second virial coefficient. Improvements to address the limitations mentioned above will be taken up in a separate work.

In the case of $\pi\,\pi \to \rho \to \pi\,\pi$, the contribution of interactions, up to the second virial level, to the entropy density can be calculated from Eq. (49) using phase shifts from the KM and BW parametrizations or phase shifts fitted to experiments where available. In Fig. 7, we contrast results of the total entropy density calculated by adding the ideal part to that from Eq. (49) using these different parametrizations of phase shifts. Again, differences arise from the parametrization of the ρ resonance in each method. It is important to mention here that the KM and BW approaches are able to take account of resonant interactions only from information on masses and widths available in the Particle Data book, but they lack consideration of repulsive channels (which are known to exist in $\pi\pi$ interactions) in many cases. In this and all subsequent figures, the hadron to quark-gluon phase transition temperature $T_c = 155 \pm 5$ MeV from the lattice calculations of the Budapest-Wuppertal collaboration [61] is shown by a rectangular box. All of our results for thermal and transport properties are meaningful only below T_c, and the results extending beyond T_c are only indicative of those in a hypothetical hadronic world.

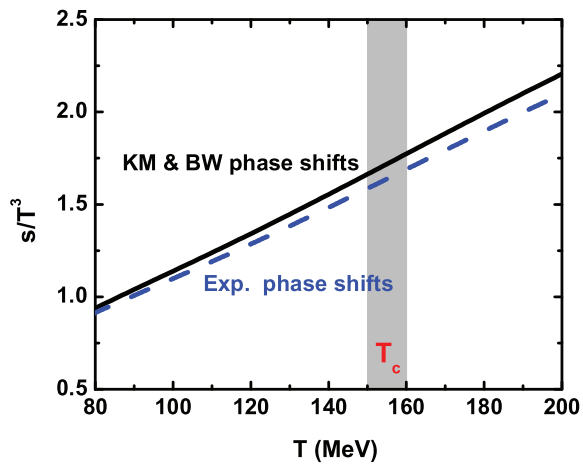

FIG. 7. (Color online) Entropy density versus temperature of pions interacting through the channel $\pi\pi \to \rho \to \pi\pi$. The dashed curve shows results when phase shifts from experiments are parameterized as in Eq. (23). The solid curve is for the K-matrix (KM) and Breit-Wigner (BW) parametrizations from Eq. (44). The transition temperature, T_c, from Ref. [61], is indicated by the rectangular box.

V. SINGLE-COMPONENT SYSTEM

Here we consider the case of a system consisting of pions only as a prototype of a single-component gas. The more realistic case of a multicomponent mixture will be considered in the next section. In Table I, we show eight resonant channels in $\pi\pi$ interactions that lead to $\pi\pi$ final states as listed in the Particle Data book [55]. Those with very small branching ratios have been omitted. With increasing temperatures, even this hypothetical single-component system is not as simple as one may first assume insofar as many resonances can and do contribute to the thermal and transport properties.

TABLE I. List of resonances formed in π-π interactions. The first column is the resonance's identity. Resonance masses (second column) and widths (third column) are in units of MeV. The last column gives the branching ratio of each decay channel. Resonances with smaller branching ratios than shown are omitted. Entries are taken from the PDG [55].

Particle	Mass (MeV)	Width (MeV)	Branching ratio π-π
ρ	774	150	1
ω	782	8	0.02
f_0	980	100	0.7
f_2	1270	185	0.875
f_{02}	1370	200	0.1
ρ_2	1465	310	0.5
$f_2^{'}$	1525	76	0.01
ρ_3	1690	235	0.1

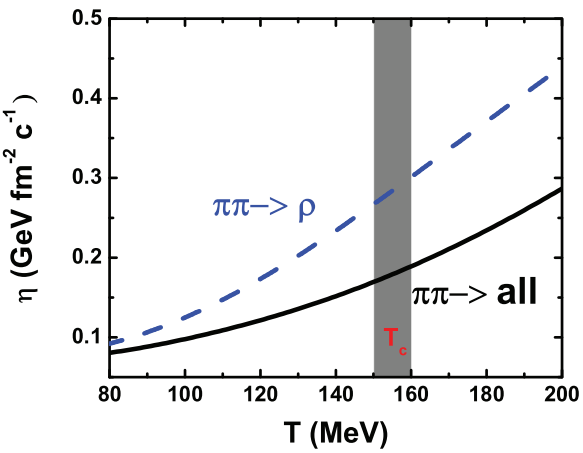

FIG. 8. (Color online) Shear viscosities (calculated by using the K-matrix formalism) vs temperature. The dashed curve shows results when only the ρ resonance was considered. Results when all possible resonances (see Table I) formed in π-π interactions were included are shown by the solid curve. The transition temperature, T_c, is indicated by the rectangular box [61].

The coefficient of shear viscosity for a single component system is calculated from Eqs. (1)–(3) for two different cases: (i) $\pi\pi \to \rho \to \pi\pi$ and (ii) $\pi\pi \to$ all channels $\to \pi\pi$. The differential cross sections for both cases are parameterized by the K-matrix formalism described in Sec. III C. The ensuing results for the shear viscosity are shown in Fig. 8. Although the ρ-meson contribution dominates, the reduction in the magnitude of the viscosity upon the inclusion of all the resonances in Table I is clearly evident, particularly close to the phase transition temperature.

The addition of more channels increases the magnitudes of thermodynamics quantities, such as the pressure, energy density, and entropy density. In Fig. 9, we show the entropy density, which is calculated by adding the ideal gas contributions to those from Eq. (49) for the $\pi\pi$ interactions. Relative

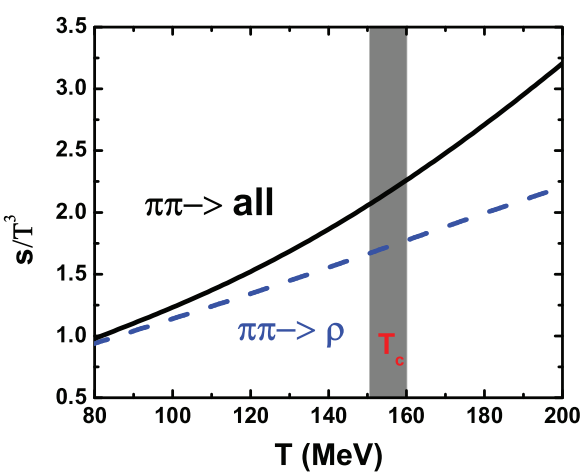

FIG. 9. (Color online) Entropy density versus temperature of an interacting pion gas. The dashed line is the result when only the ρ channel is included, whereas the solid line is the result when all resonances in Table I are included. The transition temperature, T_c, is indicated by the rectangular box [61].

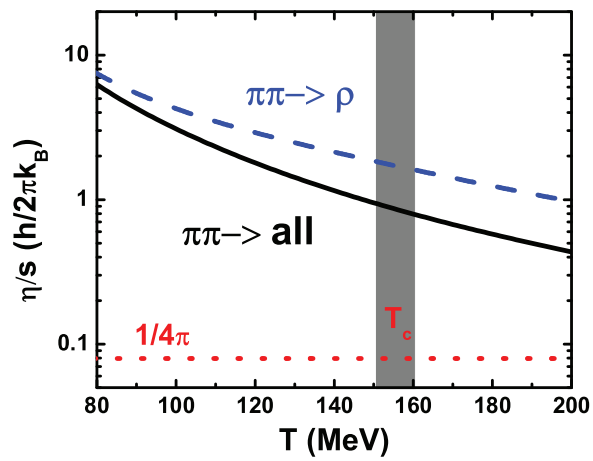

FIG. 10. (Color online) Ratio of shear viscosity (calculated using the K-matrix formalism) to entropy density versus temperature. The dashed line corresponds to the case when only the ρ resonance was considered. The solid line shows results when all possible resonances formed in π-π interactions (see Table I) were included. The AdS/CFT lower bound of η/s is shown by the red dotted line. The transition temperature, T_c, is indicated by the rectangular box [61].

to the case when only the ρ resonance is considered (dashed curve), the significant increase in the entropy density when all resonances in Table I are included (solid curve) is chiefly due to the increased number of (spin and isospin) degrees of freedom.

The ratios of η/s for the cases discussed above are shown in Fig. 10. The dashed line is the result when only the ρ channel is considered and the solid line shows the result when all resonances in Table. I are included. As the temperature approaches the hadron to quark-gluon phase transition temperature $T_c = 155 \pm 5$ MeV found in lattice simulations [61], η/s decreases more rapidly when all channels are included than when only the ρ channel is considered. The inclusion of several resonances not only causes a reduction in the coefficient of shear viscosity, η, it also results in a significant increase in the entropy density, s. Both of these effects cause the ratio η/s to become small as the temperature approaches T_c.

VI. MULTICOMPONENT SYSTEM

In this section, we consider a four-component mixture consisting of π-K-N-$\eta(548)$ and include the dominant resonances (see Tables I and II) produced in binary elastic interactions among the various constituents. In order to gain an understanding of how the inclusion of an increasing number of particles (and their associated resonances) determines the magnitudes of η and η/s, we also show results for the two-component mixtures of π-K and π-N, as well as for the three-component mixture of π-K-N together with results for the π-K-N-$\eta(548)$ mixture. Thermodynamic properties for each of the above systems, calculated using the virial expansion formalism of Sec. IV, are presented in terms of the interaction measure $I = (\epsilon - 3P)/T^4$ and compared with the lattice results of the Budapest-Wuppertal (BW) Collaboration

TABLE II. List of resonances involved in π-K-η-N interactions. The first column contains the resonance's identity. Masses (second column) and widths (third column) are in units of MeV. The remaining columns give the branching ratios of the corresponding decay channels. The data shown are from the PDG, Ref. [55].

Particle	Mass	Width	Branching ratios				
			π-K	K-K	π-η	π-N	K-N
K^*	893	50	1.0				
K_0^*	1429	287	1.0				
K_2	1430	100	0.5				
K_2^*	1410	227	0.3				
K_3^*	1680	323	0.4				
a_0	984	185		0.1	0.9		
ϕ	1020	4		0.84			
f_0^*	1370	200		0.2			
a_2	1320	107		0.05	0.14		
ϕ_2	1680	150		0.1			
ϕ_3	1890	400		0.1			
Δ_{1232}	1232	115				1.0	
Δ_{1600}	1600	200				0.15	
Δ_{1620}	1620	180				0.25	
Δ_{1700}	1700	300				0.20	
Δ_{1900}	1900	240				0.30	
Δ_{1905}	1905	280				0.20	
Δ_{1910}	1910	280				0.3	
Δ_{1920}	1920	260				0.15	
Δ_{1930}	1930	360				0.15	
Δ_{1950}	1950	285				0.45	
N_{1440}^*	1440	200				0.7	
N_{1520}^*	1520	125				0.6	
N_{1535}^*	1535	150				0.55	
N_{1650}^*	1650	150				0.8	
N_{1675}^*	1675	140				0.45	
N_{1680}^*	1680	120				0.65	
N_{1700}^*	1700	100				0.10	
N_{1710}^*	1710	110				0.15	
N_{1720}^*	1720	150				0.15	
N_{1900}^*	1900	250				0.1	
N_{1990}^*	1990	550				0.05	
Λ_{1520}^*	1520	16					0.45
Λ_{1600}^*	1600	150					0.35
Λ_{1670}^*	1670	35					0.20
Λ_{1690}^*	1690	60					0.25
Λ_{1800}^*	1800	300					0.40
Λ_{1810}^*	1810	150					0.35
Λ_{1820}^*	1820	80					0.65
Λ_{1830}^*	1830	95					0.10
Λ_{1890}^*	1890	100					0.35
Σ_{1660}^*	1660	100					0.3
Σ_{1670}^*	1670	60					0.13
Σ_{1750}^*	1750	90					0.4
Σ_{1775}^*	1775	120					0.4
Σ_{1915}^*	1915	120					0.15
Σ_{1940}^*	1940	220					0.1

[61] as well as with those of a hadron resonance gas (HRG) with the same constituents from Ref. [62].

In Fig. 11, the interaction measure I is shown for the pion gas and for the binary mixture π-K. Our results using the virial expansion method are calculated from Eqs. (47) and (48) and are shown by the solid curves. Results of the HRG model [62], calculated using the same number of particles/resonances, are shown by the dashed curves. For the pion gas, all resonances from Table I are included in both calculations. For the π-K mixture, interactions between π-π, π-K, and K-K through the resonances shown in Tables I and II are included. Note that the results from the virial expansion approach are slightly larger compared to those from the HRG model. We attribute this difference to the fact that the widths of the various resonances are accounted for naturally in the former approach whereas the HRG model includes resonances without consideration of their widths. In the limit of sufficiently small widths, the virial expansion approach guarantees that the pressure (and other thermodynamic quantities) of a dilute system of interacting particles is very well approximated by that of an ideal gas of noninteracting particles including the resonances (see Refs. [56,58,63,64]). This feature forms the basis of the HRG model. However, repulsive channels (as, for example, the δ_0^2 channel in $\pi\pi$ interactions) are not included in the HRG model. Where available, effects of repulsive channels can be straightforwardly incorporated in the virial expansion approach through the appropriate phase shifts (unfortunately, adequate data does not exist for all but the lightest mesons).

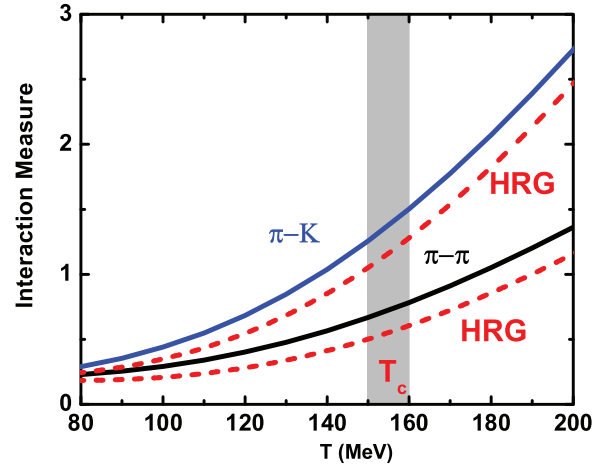

FIG. 11. (Color online) Interaction measure $I = (\epsilon - 3P)/T^4$ of interacting pions and of the mixture π-K. The solid lines are results from the virial expansion approach and the dashed lines are results from a hadron resonances gas (HRG) model [62]. The transition temperature, T_c is indicated by the rectangular box [61].

A comparison of results from the virial expansion approach to those from lattice calculations of the BW collaboration [61] is shown in Fig. 12. In the interest of being consistent with the ingredients of transport calculations, only those resonances that are formed in the π-K-η-N mixture (shown in Tables I and II) are included in the virial expansion approach. The number of resonances included in the case of the π-K-η mixture is 21 whereas 57 resonances are included in the π-K-η-N mixture. As is evident from this figure, the additional resonances present in the four-component mixture improve the agreement with the lattice results up to 140 MeV. The inclusion of additional mesons and baryons more massive than realized

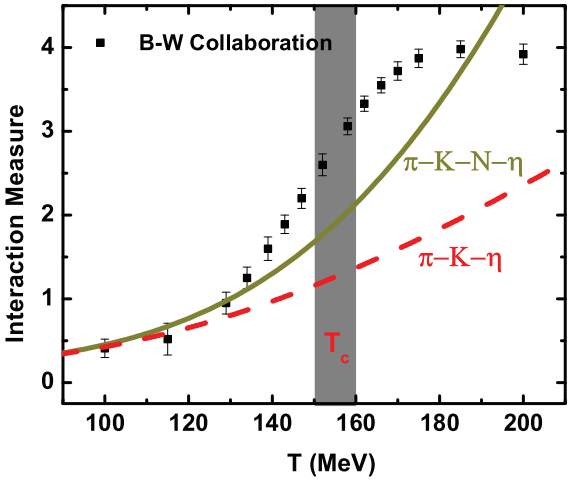

FIG. 12. (Color online) Interaction measure $I = (\epsilon - 3P)/T^4$ from lattice calculations (data points) with three- quarks ($n_f = 2+1$), $m_\pi = 135$ MeV, and lattice spacing $N_t = 8$ (BW Collaboration). The dashed line is the result for a three-component mixture of π-K-$\eta(548)$ and the solid line is the result for a four-component mixture of π-K-$\eta(548)$-N. The transition temperature, T_c, is indicated by the rectangular box [61].

in the π-K-η-N mixture is expected to improve agreement with the current lattice results (as supported by results of HRG calculations with all the resonances in the PDG book) even up to the phase transition temperature T_c [61].

The temperature dependence of the shear viscosity in a π-K-η-N mixture is displayed in Fig. 13. The progressive decrease in the magnitude of the shear viscosity with increasing temperature as more and more resonances are included is readily apparent from this figure particularly as T_c is approached. The inclusion of more resonances than considered in this work is likely to reduce the magnitude of η even further as T_c is approached (see also [65]).

The results of the ratio η/s are presented in Fig. 14. As explained in the previous section, the role of increasing the number of resonances is evident even in the case of a

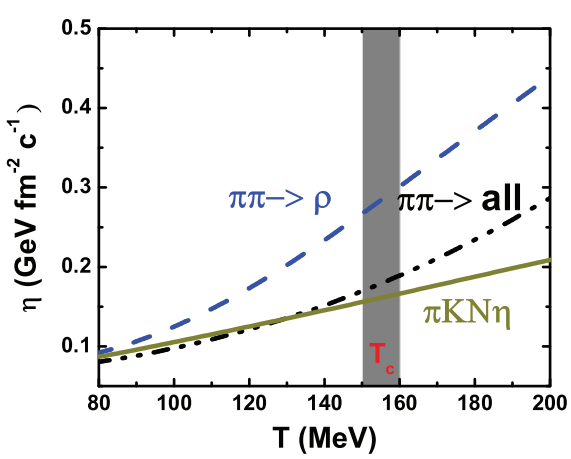

FIG. 13. (Color online) Shear viscosity vs temperature for the π-K-η-N mixture. The transition temperature, T_c, is indicated by the rectangular box [61].

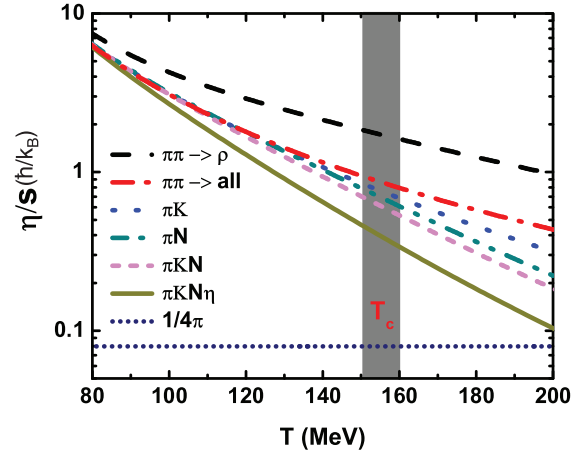

FIG. 14. (Color online) Ratio of shear viscosity to entropy density, η/s, of interacting hadrons. Results are for a single-component system (π gas), two-component mixtures (π-K and π-N), a three-component mixture (π-K-N) and a four component mixture [π-K-$\eta(548)$-N]. The horizontal curve at $1/(4\pi)$ is the AdS/CFT result.

single-component pion gas. In addition to decreasing the shear viscosity, resonances increase the entropy density both effects serving to decrease η/s with increasing temperature. A similar trend is observed in the case binary mixtures as seen from the results for the π-K and π-N mixtures. The fact that η/s for these two mixtures are nearly the same is intriguing. A physical understanding of this result resides in the masses of the resonances realized in these two systems, which are nearly the same. Results for the three (π-K-N) and four [π-K-$\eta(548)$-N] component systems highlight the increasing role of the enhanced entropy density in these systems, as the heaviest resonances are not very effective in transferring momentum in a direction perpendicular to that of fluid flow. For reference, the AdS/CFT result of $1/(4\pi)$ is also shown in this figure. From the trends seen in these results, we infer that the inclusion of additional mesons and baryons will further decrease η/s as T_c is approached, though not to the level of the AdS/CFT result.

VII. SUMMARY AND CONCLUSION

In this paper, we have calculated the shear viscosity η and the entropy density s of an interacting hadronic resonance gas. Calculations of η were performed using the relativistic generalization of the Chapman-Enskog approach, whereas calculations of the entropy density employed the relativistic virial expansion method. Our results are for a hadronic mixture with net baryon number zero and are meaningful only below the hadron to quark-gluon phase transition temperature of about 155 MeV. The mixture considered comprised of four basic hadrons π-K-η-N in which 57 resonances, formed through binary elastic interactions between the constituents, were included. In order to understand the results for the four-component mixture, calculations for a single-component pion gas, binary mixtures π-K and π-N, and the tertiary mixture π-K-η with dominant resonances were also performed. In both

the calculations of η and s, phase shifts for binary interactions among the various particles feature prominently. Experimental information on such phase shifts is only available for a few cases in the π-π, π-K, π-N, and N-N systems, but not for most of the massive resonances formed. From the masses and widths of these various resonances, phase shifts (necessary in the calculation of the thermodynamic properties of the system using the virial expansion approach) and associated differential cross sections (required in the calculation of shear viscosity using the Chapman-Enskog method) were obtained using both the Breit-Wigner (BW) and the K-matrix (KM) formalisms. For narrow and well separated resonances, both of these formalisms yield similar results that maintain unitarity of the T matrix. However, for wide and nearby resonances only the K-matrix approach preserves unitarity. The use of phase shifts and differential cross sections obtained from the K-matrix approach in the calculations of η and s is the principal new element of this work.

Our results for the single component pion gas in which eight resonances up to 1700 MeV are included highlights the important role of resonances in determining the magnitudes of η and s as a function of temperature. Increasing the number of resonances decreases the magnitude of η as additional channels of interaction are opened up, but increases s due to the increase in the number of degrees of freedom. Both these features render the ratio η/s small. These physical effects are further fortified in binary mixtures of π-K and π-N due to the presence of a large number of resonances resulting in a further decrease of the ratio η/s from the case of the single-component pion gas. Results for the tertiary mixture containing π-K-η and the four-component mixture π-K-N-η continue the trends observed in the fewer component mixtures both for η and s resulting in a much reduced ratio of η/s. The implication of these results is that were more mesons and baryons than considered in this work to be included, the ratio η/s would become even smaller than what we find here for the π-K-N-η mixture, though perhaps not to the level of the AdS/CFT result of $1/(4\pi)$ as T_c is approached.

A few future directions are suggested by our work. The inclusion of more mesons and baryons than considered here will reveal how low η/s can become in a system of hadrons with zero net baryon and strangeness numbers. To be of practical use for the low-energy scans of RHIC and other upcoming accelerators, calculations of both η and s for finite baryon and strangeness numbers appear worthwhile. Additionally, the possibility that hadrons could be far from chemical equilibrium and thus influence the magnitude of η/s needs to explored. Depending on the density and the time scales for chemical equilibration of the various species, freeze-out may occur with an overabundance of many mesons relative to the case in which full chemical equilibrium prevails. As evolution proceeds, decreasing the local density, chemical equilibrium might be lost prior to thermal equilibrium so that some constituents (e.g., pions, kaons, etc.) acquire dynamically generated chemical potentials as pointed out in Refs. [31,66,67]. Investigations of transport coefficients for multicomponent hadrons which are far from chemical equilibrium are thus worthwhile and will be taken up in future work.

ACKNOWLEDGMENTS

This work is supported by the NSFC under Grant No. 11221504, and by the US DOE under Contracts No. DE-AC02-05CH11231 and No. DE-FG02-93ER-40756.

APPENDIX A: PHASE SHIFT AND BREIT-WIGNER CROSS SECTIONS

Here, we discuss the extent to which cross sections derived from phase shifts and the Breit-Wigner parametrization are related. To be specific, we consider the process $\pi\pi \to \rho \to \pi\pi$ and its associated experimental phase shift which is parametrized as

$$\delta_1^1(\sqrt{s}) = \frac{\pi}{2} + \arctan\left(\frac{\sqrt{s} - m_\rho}{\Gamma_{\rho\to 2\pi}(\sqrt{s})/2}\right). \tag{A1}$$

The corresponding differential cross section is

$$\sigma(s,\theta) = \frac{C(I,l)}{q^2}\,\sin^2\delta_1^1\,P_1(\cos\theta), \tag{A2}$$

where $C(I,l)$ is the symmetry factor which contains spin-isospin multiplicities. We can recast the above expression to resemble the well known Breit-Wigner formula using trigonometric identities:

$$\sin(a+b) = \sin(a)\cos(b) + \cos(a)\sin(b), \tag{A3}$$

where $a = \pi/2$ and $b = \arctan[(\sqrt{s} - m_\rho)/(\Gamma_{\rho\to 2\pi}/2)]$, and

$$\cos^2(b) = \frac{1}{1+\tan^2(b)}, \tag{A4}$$

whence

$$\sin^2\delta_1^1 = \frac{1}{1+\frac{(\sqrt{s}-m_\rho)^2}{\Gamma^2_{\rho\to 2\pi}/4}} = \frac{\Gamma^2_{\rho\to 2\pi}/4}{(\sqrt{s}-m_\rho)^2 + \Gamma^2_{\rho\to 2\pi}/4} \tag{A5}$$

so that the differential cross section can be written as

$$\sigma(s,\theta) = \frac{C(I,l)}{q^2}\frac{\Gamma^2_{\rho\to 2\pi}/4}{(\sqrt{s}-m_\rho)^2 + \Gamma^2_{\rho\to 2\pi}/4}P_1(\cos\theta) \tag{A6}$$

which is the Breit-Wigner formula. However, some differences exist in the parametrizations of the widths:

$$\Gamma_{\rho\to 2\pi}(\mathrm{PS}) = 0.095\,q\left(\frac{q/m_\pi}{1+(q/m_\rho)^2}\right)^2, \tag{A7}$$

$$\Gamma_{\rho\to 2\pi}(\mathrm{BW}) = \Gamma_0\left(\frac{q}{\sqrt{s}}\right)\left(\frac{m_\rho}{q_\rho}\right)[B^1(q,q_\rho)]^2. \tag{A8}$$

Numerical values of Γ's and their total cross sections at three representative energies, $\sqrt{s} = 2m_\pi$, m_ρ, and ∞ shown in Table III serve to illustrate the differences.

TABLE III. Widths of the ρ resonance at three energies.

$\sqrt{s}$	$q/\sqrt{s}$	$\Gamma_{\rho\to 2\pi}$(PS)	$\Gamma_{\rho\to 2\pi}$(BW)	$\sigma_{\rm PS}(s)$	$\sigma_{\rm BW}(s)$
$2m_\pi$	0	0	0	0	0
m_ρ	q_ρ/m_ρ	$\Gamma_0 = 0.155$	$\Gamma_0 = 0.155$	$C(I,l)/q_\rho^2$	$C(I,l)/q_\rho^2$
∞	1/2	0	0.252	0	0

APPENDIX B: THE K-MATRIX AND BREIT-WIGNER CROSS SECTIONS

The squared T matrix can be written as

$$|T|^2 = \frac{1}{(1+K^2)^2}(K^2+K^4) = \frac{K^2}{(1+K^2)}. \tag{B1}$$

In the case of the ρ resonance, one has

$$K^2 = \frac{m_\rho^2\Gamma_{\rho\to 2\pi}^2}{\left(m_\rho^2 - s\right)^2}, \tag{B2}$$

$$(1+K^2)^2 = \frac{\left(m_\rho^2 - s\right)^2 + m_\rho^2\Gamma_{\rho\to 2\pi}^2}{\left(m_\rho^2 - s\right)^2}, \tag{B3}$$

which allows us to write

$$|T|^2 = \frac{m_\rho^2\Gamma_{\rho\to 2\pi}^2}{\left(m_\rho^2 - s\right)^2 + m_\rho^2\Gamma_{\rho\to 2\pi}^2}. \tag{B4}$$

Near the peak of the resonance,

$$m_\rho^2 - s = (m_\rho - \sqrt{s})(m_\rho + \sqrt{s}) \simeq (m_\rho - \sqrt{s})2m_\rho \tag{B5}$$

so that

$$|T|^2 = \frac{\Gamma_{\rho\to 2\pi}^2/4}{(m_\rho - \sqrt{s})^2 + \Gamma_{\rho\to 2\pi}^2/4}. \tag{B6}$$

Note that, near the peak of the resonance, the cross sections obtained from phase shifts, the Breit-Wigner formula, and the K-matrix formalism are all the same.

If the same width is used in all three parametrizations, the resulting cross sections will be identical.

APPENDIX C: K-MATRIX CROSS SECTION FOR A SINGLE RESONANCE

The differential cross section for a binary interaction is given by

$$\sigma(s,\theta)_{ab\to cd} = |f_{ab\to cd}(s,\theta)|^2, \tag{C1}$$

where $f_{ab\to cd}(s,\theta)$ is the scattering amplitude given by

$$f_{ab\to cd}(s,\theta) = \frac{1}{q}\sum_l (2l+1)T_{ab\to cd}^l(s)P_l(\cos\theta), \tag{C2}$$

with $q = 0.5\sqrt{s - 4m_\pi^2}$, l is the orbital angular momentum, $T_{ab\to cd}^l(s)$ is the interaction matrix, and $P_l(\cos\theta)$ is the orbital angular momentum dependence of the T matrix. In terms of the K matrix, the T matrix can be obtained from

$$\mathrm{Re}\,T = \frac{K}{(1+K^2)} \quad \text{and} \quad \mathrm{Im}\,T = \frac{K^2}{(1+K^2)}. \tag{C3}$$

For a resonant interaction (using the example of the ρ resonance to be specific), the K matrix can be written as

$$K = \frac{m_\rho\Gamma_{\rho\to 2\pi}}{m_\rho^2 - s}, \tag{C4}$$

where $\Gamma_{\rho\to 2\pi}$ is the width of the ρ resonance:

$$\Gamma_{\rho\to 2\pi} = \Gamma_{\rho\to 2\pi}^0\left(\frac{m_\rho}{\sqrt{s}}\right)\left(\frac{q}{q_\rho}\right)[B^1(q,q_\rho)]^2, \tag{C5}$$

where $\Gamma_{\rho\to 2\pi}^0$ is the width at the pole, $q_\rho = 0.5\,(m_\rho^2 - 4\,m_\pi^2)^{1/2}$, and the factor B is given by

$$B^1(q,q_\rho) = \frac{F_1(q)}{F_1(q_\rho)}, \tag{C6}$$

where

$$F_1(q) = \sqrt{\frac{2\,z}{z+1}}, \quad z(q) = \frac{q}{0.197}. \tag{C7}$$

APPENDIX D: TWO AND MORE RESONANCES

When two or more resonances are involved, the path through the T matrix within the K-matrix formalism becomes cumbersome, albeit straightforward. An alternative way is to use the scattering amplitude. Recall that

$$\sigma(s,\theta) = |f_{ab\to cd}(s,\theta)|^2, \tag{D1}$$

the scattering amplitude being

$$f_{ab\to cd}(s,\theta) = \sum_l^\infty (2l+1)f_l(\sqrt{s})P_l(\cos\theta) \tag{D2}$$

and

$$f_l(\sqrt{s}) = \frac{e^{i\delta_l}\sin\delta_l}{q} = \frac{1}{q}(\cos\delta_l\sin\delta_l + i\sin^2\delta_l). \tag{D3}$$

In the case of a single resonance,

$$|f_{ab\to cd}(s,\theta)|^2 = (2l+1)^2\frac{\sin^2\delta_l}{q^2}P_l^2(\cos\theta), \tag{D4}$$

while in the case of two resonances,

$$f_1 = \frac{1}{q}(\cos\delta_1\sin\delta_1 + i\sin^2\delta_1)P_1(\cos\theta), \tag{D5}$$

$$f_2 = \frac{1}{q}(\cos\delta_2\sin\delta_2 + i\sin^2\delta_2)P_2(\cos\theta). \tag{D6}$$

Resolving the scattering amplitude into its real and imaginary parts, we obtain

$$\begin{aligned}\mathrm{Re}\,f_{ab\to cd} = {} & \frac{1}{q}[(2l_1+1)\cos\delta_1\sin\delta_1 P_1(\cos\theta) \\ & + (2l_2+1)\cos\delta_2\sin\delta_2 P_2(\cos\theta)],\end{aligned} \tag{D7}$$

$$\begin{aligned}\mathrm{Im}\,f_{ab\to cd} = {} & \frac{1}{q}[(2l_1+1)\sin^2\delta_1 P_1(\cos\theta) \\ & + (2l_2+1)\sin^2\delta_2 P_2(\cos\theta)].\end{aligned} \tag{D8}$$

The generalization to more more than two resonances proceeds along similar lines as above.

[1] B. I. Abelev *et al.* (STAR Collaboration), Phys. Rev. C **81**, 044902 (2010).
[2] L. Adamczyk *et al.* (STAR Collaboration), Phys. Rev. C **86**, 054908 (2012).
[3] L. Adamczyk *et al.* (STAR Collaboration), Phys. Rev. Lett. **108**, 202301 (2012).
[4] G. Agakishiev *et al.* (STAR Collaboration), Phys. Rev. C **85**, 014901 (2012).
[5] A. Adare *et al.* (PHENIX Collaboration), Phys. Rev. Lett. **105**, 142301 (2010).
[6] A. Adare *et al.* (PHENIX Collaboration), Phys. Rev. Lett. **105**, 062301 (2010).
[7] A. Adare *et al.* (PHENIX Collaboration), Phys. Rev. Lett. **107**, 252301 (2011).
[8] A. Adare *et al.* (PHENIX Collaboration), Phys. Rev. Lett. **109**, 122302 (2012).
[9] K. Aamodt *et al.* (ALICE Collaboration), Phys. Rev. Lett. **105**, 252302 (2010).
[10] K. Aamodt *et al.* (ALICE Collaboration), Phys. Lett. B **696**, 30 (2011).
[11] K. Aamodt *et al.* (ALICE-Collaboration), Phys. Rev. Lett. **107**, 032301 (2011).
[12] K. Abbas *et al.* (ALICE Collaboration), arXiv:1303.5880.
[13] L. Milano *et al.* (ALICE Collaboration), Nucl. Phys. A **904**, 531c (2013).
[14] B. Abelev *et al.* (ALICE Collaboration), Phys. Rev. Lett. **110**, 082302 (2013).
[15] B. Hong *et al.* (ATLAS Collaboration), arXiv:1208.1615.
[16] S. Chatrchyan *et al.* (CMS Collaboration), Phys. Rev. Lett. **110**, 042301 (2013).
[17] S. Chatrchyan *et al.* (CMS Collaboration), Phys. Rev. Lett. **109**, 022301 (2012).
[18] S. Chatrchyan *et al.* (CMS Collaboration), Phys. Rev. C **87**, 014902 (2013).
[19] B. Alver and G. Roland, Phys. Rev. C **81**, 054905 (2010).
[20] L. Pang, Q. Wang, and X.-N. Wang, Phys. Rev. C **86**, 024911 (2012).
[21] H. Petersen, Phys. Rev. C **84**, 034912 (2011).
[22] M. Bleicher, K. A. Bugaev, P. Rau, A. S. Sorin, J. Steinheimer, and H. Stoecker, arXiv:1106.3647.
[23] J. Steinheimer, V. Dexheimer, H. Petersen, M. Bleicher, S. Schramm, and H. Stoecker, Phys. Rev. C **81**, 044913 (2010).
[24] C. Shen, U. Heinz, P. Huovinen, and H. Song, Phys. Rev. C **84**, 044903 (2011).
[25] T. Hirano, P. Huovinen, and Y. Nara, Phys. Rev. C **83**, 021902 (2011).
[26] H. Song and U. Heinz, Phys. Rev. C **81**, 024905 (2010).
[27] P. Romatschke and U. Romatschke, Phys. Rev. Lett. **99**, 172301 (2007).
[28] B. Schenke, S. Jeon, and C. Gale, Phys. Lett. B **702**, 59 (2011).
[29] L. P. Csernai, J. I. Kapusta, and L. D. McLerren, Phys. Rev. Lett. **97**, 152303 (2006).
[30] P. Chakraborty and J. I. Kapusta, Phys. Rev. C **83**, 014906 (2011).
[31] S. Gavin, Nucl. Phys. A **435**, 826 (1985).
[32] M. Prakash, M. Prakash, R. Venugopalan, and G. Welke, Phys. Rep. **227**, 321 (1993).
[33] J. Chen and E. Nakano, Phys. Lett. B **647**, 371 (2007).
[34] P. Arnold, G. D. Moore, and L. G. Yaffe, J. High Energy Phys. 11 (2000) 001.
[35] P. B. Arnold, G. D. Moore, and L. G. Yaffe, J. High Energy Phys. 01 (2003) 30.
[36] Z. Xu and C. Greiner, Phys. Rev. Lett. **100**, 172301 (2008).
[37] C. Wesp, A. El, F. Reining, Z. Xu, I. Bouras, and C. Greiner, Phys. Rev. C **84**, 054911 (2011).
[38] J. Chen, H. Dong, K. Ohnishi, and Q. Wang, Phys. Lett. B **685**, 277 (2010).
[39] J.-W. Chen, J. Deng, H. Dong, and Q. Wang, Phys. Rev. C **87**, 024910 (2013).
[40] P. K. Kovtun, D. T. Son, and A. O. Starinets, Phys. Rev. Lett. **94**, 111601 (2005).
[41] H. Song, S. A. Bass, and U. Heinz, Phys. Rev. C **83**, 024912 (2011).
[42] C. Gale, S. Jeon, B. Schenke, P. Tribedy, and R. Venugopalan, Phys. Rev. Lett. **110**, 012302 (2013).
[43] P. H. Polak, W. A. van Leeuwen, and S. R. de Groot, Physica **66**, 455 (1973).
[44] W. van Leeuwen, A. J. Kox, and S. de Groot, Physica A **79**, 233 (1975).
[45] W. van Leeuwen, Physica A **81**, 249 (1975).
[46] A. Wiranata and M. Prakash, Phys. Rev. C **85**, 054908 (2012).
[47] W. A. van Leeuwen, P. Polak, and S. R. de Groot, Physica **63**, 65 (1973).
[48] G. Bertsch, M. Gong, L. Mclerran, V. Ruuskanen, and E. Sarkkinen, Phys. Rev. D **37**, 1202 (1988).
[49] S. A. Bass, M. Gyulassy, H. Stöcker, and W. Greiner, J. Phys. G **25**, R1 (1999).
[50] S. U. Chung, J. Brose, R. Hackmann, E. Klempt, S. Spanier, and C. Strassburger, Ann. Phys. (NY) **507**, 404 (1995).
[51] W. M. Yao *et al.*, J. Phys. **33**, 1 (2006).
[52] J. Blatt and V. Weisskopf, *Theoretical Nuclear Physics*, 1st ed. (John Wiley & Sons, New York, 1952).
[53] E. Wigner, Phys. Rev. **70**, 15 (1946).
[54] E. Wigner and L. Eisenbud, Phys. Rev. **72**, 29 (1947).
[55] J. Beringer *et al.*, Phys. Rev. D **86**, 010001 (2012).
[56] R. Venugopalan and M. Prakash, Nucl. Phys. A **546**, 718 (1992).
[57] K. Huang, *Statistical Mechanics* (John Wiley & Sons, New York, 1963).
[58] R. Dashen, S. Ma, and H. J. Bernstein, Phys. Rev. **187**, 345 (1969).
[59] G. Welke, R. Venugopalan, and M. Prakash, Phys. Lett. B **245**, 137 (1990).
[60] E. Lu and G. D. Moore, Phys. Rev. C **83**, 044901 (2011).
[61] S. Borsanyi *et al.*, J. High Energy Phys. 11 (2010) 077.
[62] J. Steinheimer (private communication).
[63] R. Dashen and R. Rajaraman, Phys. Rev. D **10**, 694 (1974).
[64] R. Rajaraman, in *Mesons in Nuclei*, edited by M. Rho and D. Wilkinson, Vol. I (North-Holland, Amsterdam, 1979).
[65] J. Noronha-Hostler, J. Noronha, and C. Greiner, Phys. Rev. C **86**, 024913 (2012).
[66] J. L. Goity, Phys. Lett. B **319**, 401 (1993).
[67] C. Song and V. Koch, Phys. Rev. C **55**, 3026 (1997).